Modeling Interfacial Electron Transfer in the Double Layer: The Interplay between Electrode Coupling and Electrostatic Driving

Citation: Limaye, Aditya M. and Adam P. Willard, "Modeling Interfacial Electron Transfer in the Double Layer: The Interplay between Electrode Coupling and Electrostatic Driving." Journal of Physical Chemistry C 124, 2 (January 2020): 1352–1361 doi. 10.1021/acs.jpcc.9b08438 ©2019 Authors

As Published: https://dx.doi.org/10.1021/ACS.JPCC.9B08438

Publisher: American Chemical Society (ACS)

Persistent URL: https://hdl.handle.net/1721.1/128008

Version: Original manuscript: author's manuscript prior to formal peer review

Modeling interfacial electron transfer in the double layer: the interplay between electrode coupling and electrostatic driving

Aditya M. Limaye[†] and Adam P. Willard[*,‡]

[†]*Department of Chemical Engineering, MIT, Cambridge, MA*

[‡]*Department of Chemistry, MIT, Cambridge, MA*

E-mail: awillard@mit.edu

Abstract

In this manuscript we present a theoretical model for studying the population dynamics of electrochemical systems within the region of the electrical double layer. We formulate this model in a coordinate system that separately resolves both the transport of redox species in the direction perpendicular to the electrode surface and the thermal fluctuations of the solvent environment that drive electron transfer. This formulation enables us to explore how the observable characteristics of electrochemical systems are influenced by spatial variations in the electric fields and electronic couplings that are inherent to the double-layer. We apply this model to highlight the fundamental interplay between two physical attributes of interfacial electrochemistry: electrode coupling and electrostatic driving. Using a simple model system we demonstrate how variations in the location of electron transfer can lead to systematic changes to the electrochemical transfer coefficient. We also illustrate that for certain redox reactions, differences in electrostatic driving between products and reactants can lead to non-monotonic current voltage behavior.

Introduction

Electron transfer (ET) reactions at electrode-electrolyte interfaces take place within the electrical double layer (EDL), a region in which many of the physical properties that influence ET are sharply varying. Traditional models of interfacial ET reactions omit these variations by using approximations that effectively "flatten" the EDL so that it is localized to the electrode surface. In this work, we develop a model that explicitly resolves the spatial variations in the EDL and the dynamics of species within it, enabling a detailed microscopic investigation of EDL effects on interfacial ET. Our model illustrates a ubiquitous physical effect that emerges due to an interplay between electrostatic driving forces within the EDL and the spatially-dependent electronic coupling that drives interfacial ET reactions. We demonstrate that this interplay establishes an optimal location for ET, resulting in experimentally verifiable modifications to the electrochemical transfer coefficient/Tafel slope. Furthermore, we use our model to reveal the microscopic origins of the enigmatic non-monotonic current voltage behavior in peroxodisulfate electroreduction experiments, as first observed by Frumkin.[1,2] Our model is sufficiently general and easy to interpret, leaving it well-poised to offer fresh mechanistic insight into a number of additional electrochemical phenomena.

A characteristic feature of all solid-electrolyte interfaces, the EDL forms due to the preferential affinity of a specific charged species to the solid surface.[3] This preferential affinity leads to a buildup of excess charge in a region of finite width, typically 1–5 nm, that decays away from the solid surface. Across this narrow space-charge region, both the electrical potential and the electronic coupling between the reactive species and the electrode can change dramatically. Recent experimental studies have suggested that variations inside the EDL can exert significant influence on interfacial ET reactions.[4] These studies have led to numerous hypotheses about the role of EDL structure in interfacial ET reactions, however, evaluating these hypotheses requires the development of models that properly account for EDL effects.

Macroscopic transport models of electrochemical systems often assume the EDL is infinitesimally thin. Under this assumption, interfacial ET processes can be modeled using

Marcus theory,[5–7] encoded as a boundary condition by the Butler-Volmer equation,[8] or more sophisticated analogs.[9] This approach is sufficient to model some systems, but deviations from experimental behavior in others have inspired a number of empirical corrections that re-introduce EDL effects.[10–13] Continuum models with empirical EDL corrections are indispensable for engineering electrochemical devices, and will continue to find use in the quantitative interpretation of experimental results. However, reliance on *post hoc* EDL corrections hampers the ability of these models to make mechanistic remarks on the nature of ET reactions.

Electronic structure simulations, on the other hand, provide a great deal of information about the energetics of small molecular clusters near electrode interfaces. Modern density functionals can accurately predict species adsorption energies on metallic surfaces, and shed light on the preferred molecular conformations of reactive species.[14] These methods are regularly used for characterizing the thermodynamics of ET reactions, and are a useful tool for catalyst design.[15] However, electronic structure simulations typically struggle to access the characteristic length and time scales of the EDL. These scales are essential for developing a complete kinetic picture of interfacial ET processes that involve collective solvent rearrangement (e.g. with rates determined by Marcus theory).[16]

Our model operates at the intermediate length and time scales relevant to the EDL, and provides a useful complement to the previously discussed techniques. It is inspired by previous work applying reaction-diffusion equations to study the Anderson-Holstein ET model in a quasi-classical limit.[17,18] We extend these efforts by incorporating an additional reaction coordinate tracking the position of a reactive species inside the EDL. Inclusion of this electrode approach coordinate lets our model capture the effects of potential and coupling variations in the EDL, sans empirical corrections or mean-field approximations. While our model does not resolve any molecular detail or macroscopic transport phenomena, it represents the essential physics of EDL effects on interfacial ET in a natural, understandable manner. Under appropriate parametrization, our model reproduces experimental results,

and recovers the correct limiting behavior when EDL effects are unimportant.

In this paper, we start by sketching a qualitative description of the physical components of our model, followed by a presentation of its mathematical formalism. We apply this model in two different contexts. First, we study the spatial localization of ET events in the electroreduction of a neutral reactant at a cathode, and examine its impact on the electrochemical transfer coefficient. Second, we study how spatial localization of ET events depends on the applied potential in a model for peroxodisulfate electroreduction. Our results offer a compelling microscopic explanation for the non-monotonic current-voltage behavior observed in this system that is entirely consistent with contemporary macroscopic models.

Smoluchowski Master Equation (SME) Model

Reaction Coordinates

Our model resolves fluctuations along two distinct coordinates relevant to electron transfer in the EDL. The first is a Marcus coordinate, x, which tracks the collective polarization of the local dielectric solvent environment on a reactive species. In the Marcus picture,[5–7,19] the initial and final states of an ET reaction are characterized by very distinct preferred configurations of the surrounding solvent polarization field. ET events can occur when a fluctuation along a solvent polarization coordinate renders the two states roughly isoenergetic.[16,20,21] Marcus' key insight was the assumption that fluctuations along the solvent coordinate obey Gaussian statistics. The validity of Gaussian statistics (equivalently, the presence of a quadratic free energy well) in this context has been verified by numerous simulation studies, and represents a spectacular success of linear response theory.[16,22,23] In our model, x is a unitless coordinate which will house a parabolic confining free energy representing the collective preference for a species-specific solvent polarization state.

The second is an approach coordinate, z, tracking the distance of a reactive species from the electrode surface. Electrode approach is a relevant coordinate when studying interfacial

ET because numerous physical quantities affecting ET vary drastically with distance from the interface. For example, screening phenomena cause the electrostatic potential to approach its bulk value as one moves away from a constant potential interface. Additionally, the quantum mechanical electronic coupling between the reactive species and the band orbitals of the electrode changes significantly with z, serving to facilitate ET near an electrode surface. A recent study incorporated an approach coordinate to examine the interaction between interfacial ET and *macroscopic* transport processes in electrochemical devices.[24] In contrast, our model allows us to understand the influence of *microscopic* property variations and diffusive transport on interfacial ET. Hence, the approach coordinate in this model is resolved within a length scale L representing the spatial extent of the EDL, most closely associated with the Debye screening length of the electrolyte.

Free Energy Surfaces

The thermodynamics of our model are encoded into the free energy profiles of each reactive species. Specifically, we express the free energy for species i on the coordinate product space (x, z) as,

$$F_i(x, z) = \frac{k_{\text{reorg}}}{2} \left[x - \bar{x}_i\right]^2 + q_i \left[\phi(z) - \phi(0)\right] + E_{\text{int},i}. \tag{1}$$

The first term represents the (Marcus) free energy cost of deforming the solvent coordinate away from its minimum $\bar{x}_i$, where k_{reorg} specifies the width of the parabola (proportional, up to an order-one constant, to the reorganization energy). The second term represents the electrostatic energy of a point charge of magnitude q_i in an externally-applied potential $\phi(z)$. The third term is an intrinsic energy offset associated with species i. This could be due to, for example, an energetic cost for intramolecular rearrangement that accompanies an ET event.

Equation (1) requires specification of an electrostatic potential profile, $\phi(z)$, describing the manner in which screening attenuates the applied potential. A litany of models employing different assumptions about screening physics describe the functional dependence of potential

decay in the EDL.[8,25,26] The conclusions we draw from our model are insensitive to the details of the potential profile, as long as it decays to its bulk value when $z = L$. With simplicity in mind, we select a linear decay function

$$\phi(z) = V\left[1 - \frac{z}{L}\right], \tag{2}$$

where V is the applied (electrode) potential. In our model, electrostatic interactions between charged species and the potential are "one-way": species motions are influenced by the potential, but do not distort the potential profile. Physically, this corresponds to a situation in which a reactive species is dilute in an inert supporting electrolyte, a common setup for practical electrochemical measurements.

Dynamics

An ensemble of independent walkers initialized on the free energy surface of Eq. (1) and connected to a thermal bath at inverse temperature β will evolve according to Langevin dynamics. Instead of tracking the trajectories of the independent walkers, we can examine the dynamics of the entire probability distribution $P_i(x, z, t)$ as it evolves from its initial condition. In the overdamped (Brownian) limit, the distribution is propagated in time by the Smoluchowski diffusion operator[27]

$$\hat{\mathcal{L}}_i P_i \equiv \mathcal{D}\nabla \cdot \left[e^{-\beta F_i}\nabla\left(e^{\beta F_i} P_i\right)\right], \tag{3}$$

where $\mathcal{D}$ is a (scalar) diffusion constant. In the form written in Eq. (3), the Smoluchowski operator implicitly obeys the fluctuation-dissipation theorem. In terms familiar to electrochemical literature, Eq. (3) takes advantage of the Nernst-Einstein relation to parametrize electromigrative drift and diffusion rates by a *single* diffusion constant.[8]

In addition to diffusing on its own free energy surface, a member of species i can also undergo an outer-sphere ET event to transform into a different species j. This type of ET

phenomenon is inherently quantum mechanical, and involves a switch between two Born-Oppenheimer surfaces near a diabatic crossing point. A full quantum dynamical description of the diabatic intersection is outside the scope of this study. However, we can extract information about the resultant occupation statistics on the two diabatic surfaces using surface hopping (SH) dynamics. Under the SH picture, a walker can "hop" between surfaces at a rate proportional to the electronic coupling. In terms of distributional evolution, SH dynamics can be modeled with a master equation approach which includes continuous balanced sink/source rates that transform one species to another, effectively connecting free energy surfaces. This approach has been used heuristically[28–30] and also developed rigorously[17,18,31] in prior work on interfacial ET.

The sink and source rates must be set such that the stationary distribution of the dynamics respects the proper equilibrium (Boltzmann) distribution. There is, in principle, no unique way to define these rates, but a simple expression for the sink/source rate between surfaces i and j in accordance with prior work[17,32] is,

$$\zeta_{i\to j}(x,z) = \frac{\Gamma_{ij}(z)}{\hbar} f\left[F_j(x,z) - F_i(x,z)\right], \tag{4}$$

where $f[\cdot]$ is the Fermi distribution of the electrode. The coupling profile, $\Gamma_{ij}(z)$, changes upon electrode approach, primarily because of increasing overlap between the molecular orbitals of the redox species and the band orbitals of the electrode.[33] Previous studies on ET[28,33–37] and self-assembled monolayers[38,39] have used the exponential form,

$$\Gamma_{ij}(z) = \bar{\Gamma}_{ij} \exp\left[-z/z_{\mathrm{dec},ij}\right], \tag{5}$$

for this decay, consistent with detailed quantum mechanical calculations.[40–42] Prior studies report a wide range of values for $\bar{\Gamma}_{ij}$ and $z_{\mathrm{dec},ij}$, suggesting that they are dependent on the chemical details of the system. Hence, the coupling magnitude and decay rate are important physical parameters in our model, and we thoroughly examine the effects of varying them

within reasonable values. We note that Eq. (5) neglects any dependence of the coupling on the applied electrode potential, though this effect may play an important role at high electrode surface charge density.[35]

Conservation of probability mass yields the following set of coupled partial differential equations describing the dynamics of the species population distributions,

$$\frac{\partial P_i}{\partial t} = \hat{\mathcal{L}}_i P_i + \sum_{j \neq i} \left[\zeta_{j \to i} P_j - \zeta_{i \to j} P_i \right]. \tag{6}$$

For numerical and analytical convenience, we will non-dimensionalize Eq. (6) utilizing the EDL length scale L and the diffusive timescale $\tau \equiv L^2/\mathcal{D}$. The scaled spatial coordinate, time, hopping rate, and propagator are given by $\tilde{z} = z/L$, $\tilde{t} \equiv t/\tau$, $\tilde{\zeta}_{i \to j} \equiv \tau \cdot \zeta_{i \to j}$, and $\hat{\tilde{\mathcal{L}}} \equiv \tau \cdot \hat{\mathcal{L}}$, respectively. Full details on the non-dimensionalization procedure are described in the SI. From here on, we will drop all tildes, and work exclusively with the non-dimensional variables. Taken together, these equations comprise a Smoluchowski master equation (SME) that describes the distributional evolution of our reactive ensemble.

Boundary Conditions

Finally, we need to specify appropriate boundary conditions on Eq. (6). We would like to use the SME to determine the amount of current passed from the electrode in a non-equilibrium steady state (NESS) defined by a particular applied voltage V. The NESS is created by maintaining a constant probability density (equivalently, a concentration) of reactant species and a vanishing probability density of product species at the EDL boundary ($z = 1$). Both probability densities are equilibrated with respect to the Marcus coordinate x at the EDL boundary. In a real system, these concentrations could be maintained by fast convective mass transport mechanisms (vigorous stirring, a rotating-disk electrode, etc.). It is worth noting that many electrochemical phenomena of interest (cyclic voltammetry peaks,[43] Sand's time,[44] etc.) are the result of slow external mass transport processes influencing interfacial

ET rates. Assessing the effects of external mass transfer limitations is outside the scope of this work, but it is easy to imagine a multi-scale scheme that couples the SME dynamics described here to a macroscopic transport model.[45]

We consider the electrode surface at $z = 0$ to be ideally blocking; it does not admit species adsorption or intercalation, implying a no-flux boundary condition for all species. Because of the strongly confining Marcus potential in the x coordinate, with sufficiently large domains, it is largely immaterial whether we specify a zero-concentration or a no-flux boundary condition at the x-boundaries. For computational convenience, we choose to specify no-flux boundary conditions. The boundary conditions uniquely specify a steady-state solution to Eq. (6), which we compute numerically. Various properties of the NESS (current, preferred position of ET, etc.) can be computed using the numerical steady-state solution. Computational details on our solution scheme can be found in the SI.

Spatial Localization of ET

The electrode approach coordinate z mediates a physical tradeoff that is germane to nearly all interfacial electrochemistry. Due to the decay of the potential $\phi(z)$ (as modeled by Eq. (2)), the driving force for ET is greatest further from the electrode. At the same time, the electronic coupling that facilitates ET decays with z (as modeled by Eq. (5)), achieving its greatest value at the electrode surface. The competition between these two effects leads to an optimal/modal position for ET, with experimentally-measurable consequences. Here, we evaluate these consequences with a simple model.

Model Specification

The simplest possible model system exhibiting this behavior is the case of a netural species (species 0) being reduced in a single-electron outer-sphere reaction to produce a negatively charged species (species 1). Due to its simplicity, this model is excellent for gaining an

intuitive understanding of the SME, and also showcases the effects of changing the $\bar{\Gamma}_{01}$ and $z_{\mathrm{dec},01}$ parameters of the coupling profile. We select parameters that are in line with typical electrochemical reactions, choosing $E_{\mathrm{int},0} = 0$ eV, $E_{\mathrm{int},1} = 0.20$ eV, $k_{\mathrm{reorg}} = 1$ eV, and $T = 300$ K. We study the current-voltage behavior of this system by varying the applied voltage V across a broad range of tunings of the parameters $\bar{\Gamma}_{01}$ and $z_{\mathrm{dec},01}$. All conclusions derived from this model are relatively insensitive to properly-correlated changes in the selected parameters.

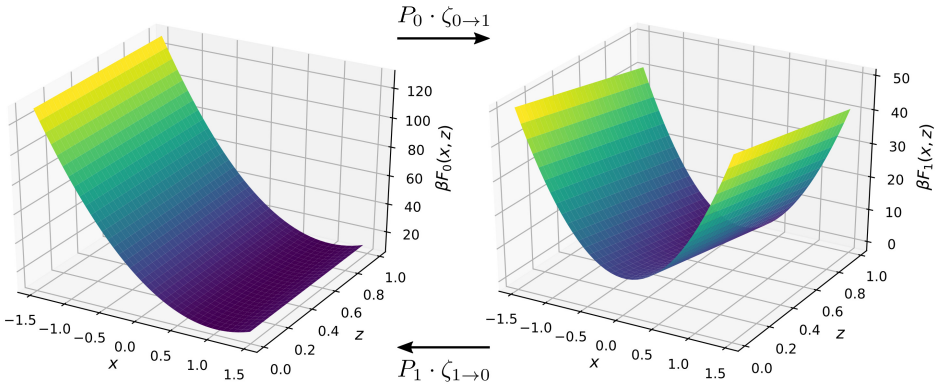

Figure 1: Free energy profiles computed from Eq. (1) for a simple two-species model.

Figure 1 shows free energy profiles for both species when the electrode is held at $V = -0.25$ V. Because species 0 carries no charge, its free energy has no electrostatic contribution, and is independent of the approach coordinate. The free energy for species 1, however, exhibits a strong dependence on the approach coordinate. At $z = 1.00$, the reduced state is favored energetically by 50 meV, a driving which vanishes entirely at $z = 0.80$ due to decay of the electrical potential in the EDL. Our model is equivalent to a traditional Marcus theory description at the $z = 1$ spatial slice, where changing the applied potential by an amount δV shifts the driving force by exactly δV. For $z < 1$, a region not considered in traditional Marcus theory, screening causes the driving force to shift by an amount *strictly less* than δV.

Mapping ET Location

Our model resolves where ET events occur along the electrode approach coordinate. In the NESS, there will be a net current between states, which can be quantified as a function of the Marcus coordinate and the approach coordinate by the following observable:

$$\Delta(x,z) \equiv \frac{\zeta_{0\to1}P_0 - \zeta_{1\to0}P_1}{\int\int \mathrm{d}x\mathrm{d}z\,[\zeta_{0\to1}P_0 - \zeta_{1\to0}P_1]}. \tag{7}$$

This observable essentially describes the flux of population between the two states occurring at a specific point in coordinate space. In the case of traditional Marcus theory, the reaction occurs only at the EDL boundary, implying $\Delta(x,z) = \delta[x-x^*]\cdot\delta[z-1]$, where $\delta[\cdot]$ denotes a Dirac delta function, and x^* denotes the value of x where the parabolas cross. The SME model improves on traditional Marcus theory by resolving the electrode approach coordinate. In order to isolate the z-dependence, we marginalize over the Marcus coordinate:

$$\bar{\Delta}(z) \equiv \int \mathrm{d}x\ \Delta(x,z). \tag{8}$$

Since the EDL thickness L sets the length scale of our model, changes in the electrostatic screening length or the decay length of the coupling profile are equivalently described by varying the $z_{\mathrm{dec},01}$ parameter.

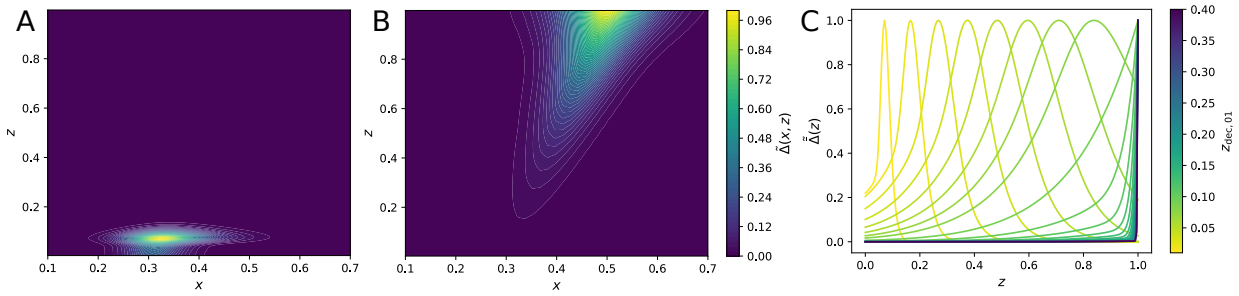

Figure 2: Mapping the spatial localization of electron transfer. (A, B) Spatial maps of $\Delta(x,z)$ for $z_{\mathrm{dec},01} = 0.01$ and $z_{\mathrm{dec},01} = 0.10$, respectively. (C) Traces of the normalized marginal current $\bar{\Delta}(z)$ for values of $z_{\mathrm{dec},01} \in [0.01, 0.40]$.

Figure 2 depicts the effects of changing $z_{\mathrm{dec},01}$ on $\Delta(x,z)$ when $\bar{\Gamma}_{01} = 6$ eV. Figure 2A illustrates that when the coupling profile decays quickly, electron transfer only occurs within a short distance of the electrode surface. Here, the driving force is much smaller than the applied voltage. Figure 2B illustrates that when the coupling profile decays gradually, the electron transfer peaks at z-values further away from the electrode. Here, the driving force is higher, approaching the applied voltage. Figure 2C depicts profiles of $\bar{\Delta}(z)$ as a function of the coupling decay parameter $z_{\mathrm{dec},01}$, each independently normalized. We observe that the width of the profiles increases as $z_{\mathrm{dec},01}$ increases, indicating that ET is occuring over a broader region of space. At extremely high values of $z_{\mathrm{dec},01}$, the SME model collapses to traditional Marcus theory, since all ET events are localized to $z = 1$. Physically, this corresponds to a situation where the electrolyte screening length is considerably smaller than a typical electronic tunneling distance. This matches expectation – traditional Marcus theory is known to work well for pure outer-sphere interfacial electrochemistry, where electrons tunnel from electrode to species through the entire EDL.[10]

Transfer Coefficients

Variation in the location of ET within the EDL can precipitate measurable changes in the transfer coefficient α. The transfer coefficient is defined by the empirical Butler-Volmer current-voltage relationship for a cathodic reaction,[8]

$$i = i_0 \exp\left\{\alpha \cdot \beta \left[-eV - \Delta E_{\mathrm{int}}\right]\right\}, \tag{9}$$

where i is the measured current density, i_0 is the zero-potential (exchange) current density, e is the fundamental charge unit, and $\Delta E_{\mathrm{int}} \equiv E_{\mathrm{int},1} - E_{\mathrm{int},0}$. The underpinnings of Marcus kinetics[16] imply the Arrhenius relationship,

$$i = i_0 \exp\left[-\beta E_a\right],$$

where E_a is the activation energy. Hence, the transfer coefficient α must obey the relationship,

$$\alpha = -\left[\frac{\partial E_a}{\partial(eV)}\right]. \tag{10}$$

In plain terms, α quantifies the amount that an externally-applied voltage V changes the activation energy, and hence the observed current. Up to appropriate unit scalings, the transfer coefficient is the inverse of the Tafel slope, another quantity often resolved in electrochemical measurements. Traditional Marcus theory offers the following prediction for the dependence of α on the applied potential (see SI for a detailed derivation):

$$\alpha_{\text{Marcus}} = \left[\frac{1}{2} + \frac{\Delta E_{\text{int}} + eV}{k_{\text{reorg}}}\right]. \tag{11}$$

Equation (11) implies that at the equilibrium potential $V_{\text{eq}} = -\Delta E_{\text{int}}/e$, the transfer coefficient should be exactly 1/2, then decrease with more cathodic applied potentials, eventually becoming negative at potentials below $-\left(k_{\text{reorg}} + 2\Delta E_{\text{int}}\right)/2e$, corresponding to the Marcus inverted regime. Thus, the expectation for typical outer-sphere electrochemical reactions is that the transfer coefficient decreases from $\alpha = 1/2$ as the potential is tuned from V_{eq} to more negative values.

Figure 3 shows current-voltage measurements for several different values of the coupling localization parameter $z_{\text{dec},01}$, holding $\bar{\Gamma}_{01} = 6$ eV. Transfer coefficients are determined by simple linear regression to the initial region of the curves, and are plotted as solid circles in Fig. 3B. Counter to expectation, at low values of $z_{\text{dec},01}$, the equilibrium potential transfer coefficients predicted by the model are significantly smaller than the Marcus theory prediction of 1/2. The attenuated transfer coefficients are a direct consequence of the driving force/coupling strength tradeoff in the z-coordinate. For small $z_{\text{dec},01}$ values, ET can only occur within a short distance from the electrode surface, where the potential deviates very little from the electrode potential (and hence the electrostatic driving force is very low). Due to this "pinning" effect, increasing the applied potential has less of an effect on the activation

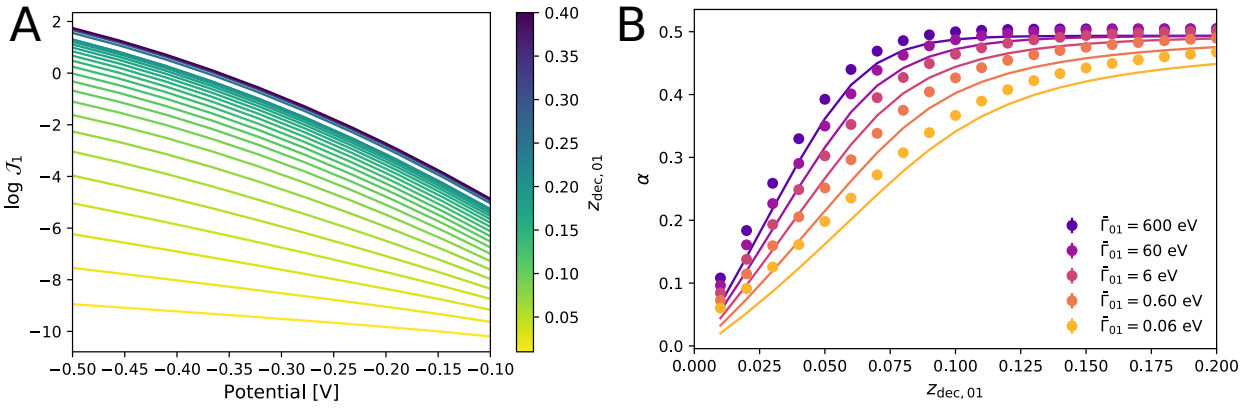

Figure 3: Current-voltage curves and transfer coefficient predictions from the two-surface model. (A) Several current-voltage curves measured for different values of the coupling localization parameter $z_{\mathrm{dec},01}$, with $\bar{\Gamma}_{01} = 6$ eV. (B) Transfer coefficients determined by linear fitting for a number of different coupling strengths are shown as colored dots. The solid lines are predictions from the simple model/approximation developed in Eq. (14).

energy of the reaction compared to the case where the reaction occurs at the EDL boundary $z = 1$ (see SI for schematic illustration).

We can devise a simple approximation for the functional dependence of the transfer coefficient α on $z_{\mathrm{dec},01}$ by leveraging information contained in the net current profile $\Delta(x, z)$. Given that ET occurs at any value of z, the activation energy is now a function of the approach coordinate, with a profile denoted as $E_a(z)$. The average activation energy $\langle E_a \rangle$ can be determined by integrating $E_a(z)$ against the empirical marginal of the net current,

$$\langle E_a \rangle = \frac{\int \mathrm{d}z \; \bar{\Delta}(z) E_a(z)}{\int \mathrm{d}z \; \bar{\Delta}(z)}. \tag{12}$$

Equations (1) and (2) yield the following expression (see SI for complete derivation) for the activation energy profile,

$$E_a(z) = \frac{k_{\mathrm{reorg}}}{2} \left[\frac{1}{2} + \frac{\Delta E_{\mathrm{int}} + eVz}{k_{\mathrm{reorg}}} \right]^2. \tag{13}$$

Assuming that the net current profile is roughly independent of the applied potential, ap-

plying the Leibniz rule yields,

$$\alpha = -\int \mathrm{d}z \; \tilde{\bar{\Delta}}(z) \cdot \left[\frac{\mathrm{d}E_a}{\mathrm{d}(eV)}\right] \;, \tag{14}$$

where $\tilde{\bar{\Delta}}(z)$ denotes $\bar{\Delta}(z)$ normalized by its own integral. The solid lines in Fig. 3B are constructed from numerical evaluation of Eq. (14), and match the qualitative behavior of the measured α quite well. However, Eq. (14) assumes a limit of small coupling, resulting in systematic underestimation of the measured α values. The non-adiabatic hopping expression used in the SME model enables transitions away from the parabola crossing, thus increasing the measured α value. When this smearing effect is reduced by increasing k_{reorg}, the predictions from Eq. (14) achieve quantitative agreement with the measured α values from the SME model (see SI).

Implications

The variation of the preferred electron transfer position in z with changes in the $z_{\mathrm{dec},01}$ parameter has implications for the analysis of current-voltage behavior for outer-sphere ET reactions. Current-voltage curves are typically fit to Eq. (9), which predicts an exponential dependence between the the observed current and the *applied* potential. This relationship can only hold if all ET events occur at $z = 1$, and should fail spectacularly for ET events that are localized much closer to the interface, where the reaction potential is much lower in magnitude than the applied potential.

A correction to the Butler-Volmer equation developed by Frumkin accounts for this effect by adjusting the driving force to the mean potential at the most likely transition state (TS) position (termed "psi-prime" in the original literature).[46,47] Frumkin originally set the psi-prime potential to the potential at the outer Helmholtz plane (OHP). Disagreements with experimental results inspired a number of studies that expanded on Frumkin's formalism, but they all preserve the assumption that the most likely reaction site is at the OHP.[48–51]

We note that there is no *a priori* basis to assume that the most likely position for the ET event is exactly at the OHP. We demonstrate that this position can be fuzzy, and intricately dependent on molecular details of the redox species (coupling profile with an electrode), as well as on electrolyte characteristics (screening length).

If the typical position of ET is within the region of potential decay in the EDL, then there are additional implications for the measured transfer coefficient. In particular, we show that transfer coefficients can be significantly lower than the traditional Marcus prediction of 1/2 for reactions that occur inside the EDL. Previous studies[52–56] have speculated about the effects of changing reaction site position on the transfer coefficient; the SME model presented here confirms this speculation in a quantitative manner. This phenomenon provides a plausible explanation for the unusually high Tafel slopes observed for certain outer-sphere reactions such as ammonia oxidation.[57]

Potential Dependence of Spatial Localization

The model discussed in the previous section involves the reduction of a neutral species, which is completely unresponsive to electrostatic forces in the EDL. In this case, we find empirically that the optimal position for ET is roughly independent of the applied potential. However, it is often the case that both the oxidized and reduced species are ionic, and thus both responsive to electrostatic forces in the EDL. Since these forces depend on the applied potential, changes in the potential can change the modal position of ET, yielding experimentally-measurable consequences.

Background

The effects of electrostatic repulsion from an electrode on current-voltage behavior are often treated using Frumkin's correction to the Butler-Volmer equation. In textbook form,[8] the

correction reads,

$$i_{0,\mathrm{obs}} = \exp\left[\beta\left(e\alpha - q_{\mathrm{ion}}\right)\phi(z_{\mathrm{rxn}})\right] \cdot i_{0,\mathrm{true}}, \tag{15}$$

where q_{ion} is the charge carried by the ionic reactant species, z_{rxn} is the most likely position of the reaction, and $\phi(z_{\mathrm{rxn}})$ is the electrostatic potential at this position. Equation (15) packages the driving force correction mentioned previously with another correction describing the attenuation (magnification) of the species concentration due to electrostatic repulsion (attraction). To understand the implications of this equation, consider the electroreduction of an anionic species at a cathodic applied potential. If z_{rxn} is far from the electrode (near the EDL boundary), the Frumkin correction will be small, because $\phi(z_{\mathrm{rxn}})$ should be nearly zero (the bulk potential), leading to roughly unperturbed Butler-Volmer current-voltage behavior. On the other hand, if z_{rxn} is very close to the electrode, the Frumkin correction shuts off all current at cathodic voltages, because electrostatic repulsion of the anion depletes its concentration at z_{rxn}. In all cases, if z_{rxn} is assumed constant over a linear voltage sweep, Eq. (15) predicts monotonic current-voltage behavior – depending on the value of q_{ion}, the current could either uniformly increase or decrease over the sweep.

Frumkin and others did a number of experiments[2,46,58] on the electroreduction of the peroxodisulfate anion in the following cathodic half-reaction:

$$\mathrm{S_2O_8}^{2-} + 2\,\mathrm{e}^- \longrightarrow 2\,\mathrm{SO_4}^{2-}. \tag{16}$$

Unexpectedly, experiments consistently observe non-monotonic "S"-shaped current-voltage behavior. When tuning from low to high cathodic voltages, the current increases and goes through a maximum, at which point it begins to descend steeply and then goes through a minimum, and then continues to increase for the rest of the scan range (see Figure 1 of Frumkin et al.[2]). This unusual behavior is only observed in a handful of systems that feature the reduction of a large anionic species carrying a high charge.[1] The prevailing physical explanation for this phenomenon relies on electrostatic forces in the EDL.[2] The initial

increasing current branch occurs at cathodic potentials below the potential of zero charge (pzc) of the electrode. In this voltage regime, the electrode carries a slightly positive surface charge, which interacts favorably with the anionic reactive species; the current increases with voltage according to Eq. (9). The subsequent current decrease occurs upon crossing the pzc, when the negatively charged surface generates electrostatic repulsion that attenuates the current in the manner described by Eq. (15). The current minimum and following increase at even more cathodic potentials has proven difficult to rationalize experimentally.[51]

Much of the literature on peroxodisulfate electroreduction focuses on explaining the dependence of specific features in the "S"-shaped current-voltage curves on the concentrations of different spectator ions.[59–61] Our model resolves the "S"-shape without invoking molecular detail, suggesting that distance-dependent electrostatic driving and coupling alone are sufficient to explain this anomalous behavior.

Model Specification

The peroxodisulfate electroreduction reaction maps naturally to a two-surface model that includes an anionic species (species 0) carrying charge $q_0 = -1$ and another anionic species (species 1) carrying charge $q_1 = -2$. For convenience, we assign parameter values $E_{\text{int},0} = 0$ eV, $E_{\text{int},1} = 0.05$ eV, $k_{\text{reorg}} = 1$ eV, and $T = 300$ K. For these fixed parameter values, we study current-voltage behavior over a range of $z_{\text{dec},01}$ values.

Changing $z_{\text{dec},01}$ could correspond to altering the electrostatic screening length in the solution or modifying the species/surface chemistry, altering the spatial localization of the electronic coupling. Our model does not resolve the presence of specific ions in the EDL other than the redox-active species, implying that the "pzc" in our model coincides with the point of zero applied potential, $V = 0$. Figure 4 depicts the species free energy profiles when the electrode is held at $V = -0.25\,\text{V}$. Both species carry a charge, and hence both free energy surfaces depend on the approach coordinate.

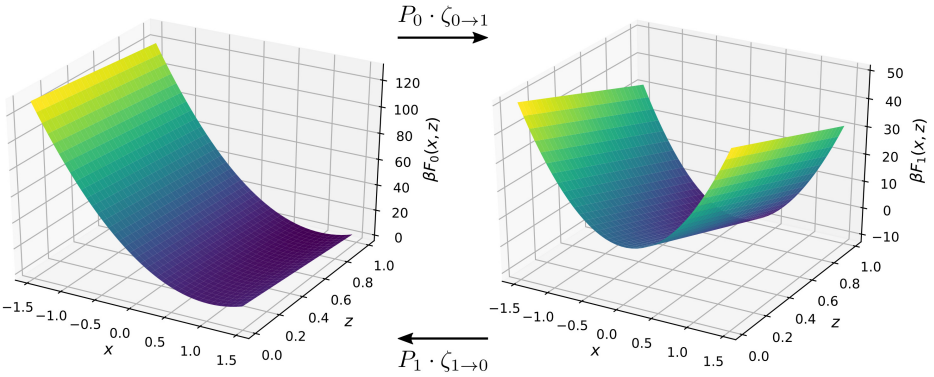

Figure 4: Free energy profiles computed from Eq. (1) for a model mapping to the peroxodisulfate reduction system in Eq. (16)

Understanding S-Shaped Current-Voltage Behavior

Figure 5A depicts current-voltage curves over a range of values of $z_{\mathrm{dec},01}$. Our model recovers "S"-shaped current-voltage behavior as observed by Frumkin for a limited range of values of $z_{\mathrm{dec},01} \in [0.06, 0.09]$. On either side of this region, we see very different asymptotic behavior. For $z_{\mathrm{dec},01} > 0.09$, electrostatic repulsion effects contribute only a small kink in the current-voltage behavior. Figure 5B confirms that in this case, the current continues to increase exponentially at more cathodic potentials, flattening only due to the effects of the avoided inverted region in Marcus kinetics at an electrode. For $z_{\mathrm{dec},01} < 0.06$, on the other hand, electrostatic repulsion effects strongly influence the current-voltage behavior, leading to negative transfer coefficients that eventually approach zero at far more cathodic potentials.

This behavior can be rationalized in the context of Eq. (15) by assuming that z_{rxn} depends on the applied potential. This dependence is not considered in the original Frumkin treatment, and is a unique consequence of the interplay between electrostatic repulsion and distance dependent driving/coupling. Since the SME model gives us direct access to spatial map of ET events, we can define

$$\langle z \rangle_{\mathrm{rxn}} \equiv \int \mathrm{d}z \cdot z \cdot \tilde{\tilde{\Delta}}(z), \tag{17}$$

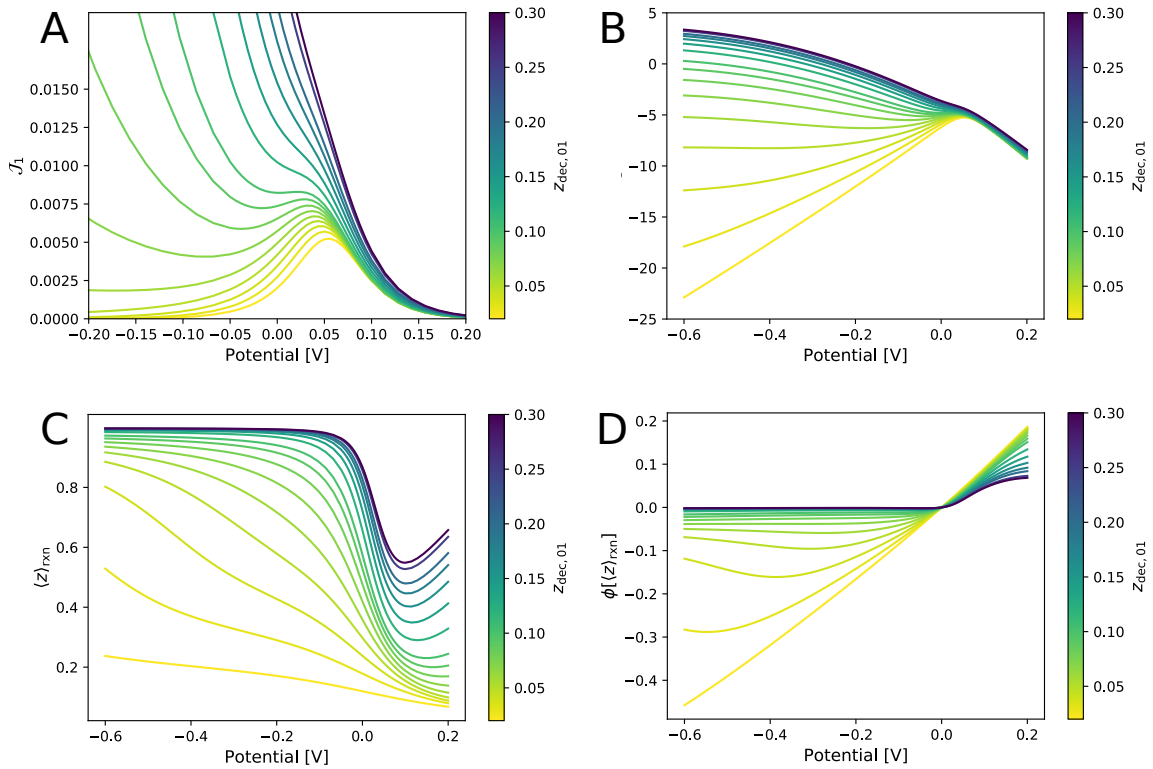

Figure 5: Results from model mapped to peroxodisulfate reduction. (A) Current-voltage curves computed for a family of models with different $z_{\mathrm{dec},01}$ values. (B) Same data as in top left, but the current is plotted on a logarithmic scale, enabling the simple identification of regions with positive and negative Tafel slopes. (C) Traces of the most likely site for electron transfer, determined from the mean value of $\Delta(x, z)$, defined in Eq. (7) as a function of the applied potential, for various values of $z_{\mathrm{dec},01}$. (D) Traces of the electrostatic potential at the most likely site for electron transfer, a value that plays an operative role in the Frumkin correction in Eq. (15).

where $\langle z \rangle_{\mathrm{rxn}}$ denotes the *mean* position for ET. Unlike in the case of the neutral reactant species, Fig. 5C demonstrates that $\langle z \rangle_{\mathrm{rxn}}$ is indeed a function of the applied potential. Cathodic of the pzc, $\langle z \rangle_{\mathrm{rxn}}$ increases with applied voltage for all values of $z_{\mathrm{dec},01}$, since the reactant is repelled from the negatively-charged electrode surface. However, due to distance-dependent coupling, the rate of increase depends strongly on the value of $z_{\mathrm{dec},01}$. At high $z_{\mathrm{dec},01}$, the ET reaction is facile even far away from the electrode, so $\langle z \rangle_{\mathrm{rxn}}$ quickly reaches the EDL boundary, where electrostatic repulsion is minimized and driving force is maximized. For low $z_{\mathrm{dec},01}$, the ET reaction is very sluggish at large z, so $\langle z \rangle_{\mathrm{rxn}}$ creeps away from the electrode surface slowly. The effects of changing $\langle z \rangle_{\mathrm{rxn}}$ as a function of applied potential are observed clearly in Fig. 5D, which tracks $\phi\left(\langle z \rangle_{\mathrm{rxn}}\right)$ as a function of the applied potential. Non-monotonic current-voltage behavior occurs when $\phi\left(\langle z \rangle_{\mathrm{rxn}}\right)$ goes through a minimum, demarcating a switch between an increasing and decreasing Frumkin correction.

Implications

Results from the SME model suggest that the striking "S"-shaped behavior observed in the peroxodisulfate electroreduction experiments is best contextualized on a continuum parametrized by $z_{\mathrm{dec},01}$, a dimensionless quantity relating the length scales for electronic tunneling and electrostatic screening. When the tunneling length scale is much larger than the screening length scale, the Frumkin correction is negligible, consistent with experimental results for reactions involving electron tunneling through the entire EDL.[10,62] When the tunneling length scale is much smaller than the screening length scale, electrostatic repulsion dominates and shuts off ET, since the reactant cannot approach close enough to couple to the band orbitals of the electrode. When the two scales are delicately balanced, electrostatic repulsion effects initially reduce the current, until the potential driving force is large enough to drive ET entirely at the EDL boundary. The microscopic insight provided by the SME model is consistent with modern work on peroxodisulfate reduction, which has argued that the current increase at highly cathodic potentials is due to broadening of the "reaction zone"

over which ET may occur.[51] In fact, prior studies have speculated that the most likely transition state position for peroxodisulfate reduction can deviate from the OHP position as a function of applied potential.[10,62–64] Our model provides quantitative confirmation for this hypothesis.

Acknowledgement

The authors thank Zachary Schiffer, David Koshy, Yogi Surendranath, Joe Subotnik, Sharon Hammes-Schiffer, and Karthish Manthiram for useful discussions. This material is based upon work supported by the Air Force Office of Scientific Research (AFOSR) under award number FA9550-18-1-0420. AW acknowledges the Research Corporation for Scientific Advancement (Cottrell Scholar) and AY acknowledges a graduate research fellowship from the National Science Foundation.

Supporting Information Available

Additional model details, specifics of numerical solution implementation, complete derivations of analytical results, and parametric sensitivity analyses.

References

(1) Frumkin, A.; Nikolajeva, N. On the electroreduction of anions. *The Journal of Chemical Physics* **1957**, *26*, 1552–1553.

(2) Frumkin, A.; Nikolaeva-Fedorovich, N.; Berezina, N.; Keis, K. E. The electroreduction of the S2O82- anion. *Journal of Electroanalytical Chemistry and Interfacial Electrochemistry* **1975**, *58*, 189–201.

(3) Bockris, J. O.; Reddy, A. K. *Modern electrochemistry 2B: electrodics in chemistry,*

engineering, biology and environmental science; Springer Science & Business Media, 2000; Vol. 2.

(4) Chen, L. D.; Urushihara, M.; Chan, K.; Nørskov, J. K. Electric Field Effects in Electrochemical CO ₂ Reduction. *ACS Catalysis* **2016**, *6*, 7133–7139, DOI: 10.1021/acscatal.6b02299.

(5) Marcus, R. A. On the theory of oxidation-reduction reactions involving electron transfer. I. *The Journal of Chemical Physics* **1956**, *24*, 966–978.

(6) Marcus, R. A. Theory of oxidation-reduction reactions involving electron transfer. 4. A statistical-mechanical basis for treating contributions from solvent, ligands, and inert salt. *Discussions of the Faraday Society* **1960**, 21–31.

(7) Marcus, R. A. Chemical and electrochemical electron-transfer theory. *Annual review of physical chemistry* **1964**, *15*, 155–196.

(8) Bard, A. J.; Faulkner, L. R.; Leddy, J.; Zoski, C. G. *Electrochemical methods: fundamentals and applications*; wiley New York, 1980; Vol. 2.

(9) Chidsey, C. E. D. Free Energy and Temperature Dependence of Electron Transfer at the Metal-Electrolyte Interface. *Science* **1991**, *251*, 919–922, DOI: 10.1126/science.251.4996.919.

(10) Gavaghan, D. J.; Feldberg, S. W. Extended electron transfer and the Frumkin correction. *Journal of Electroanalytical Chemistry* **2000**, *491*, 103 – 110, DOI: https://doi.org/10.1016/S0022-0728(00)00210-2.

(11) Kilic, M. S.; Bazant, M. Z.; Ajdari, A. Steric effects in the dynamics of electrolytes at large applied voltages. II. Modified Poisson-Nernst-Planck equations. *Physical Review E* **2007**, *75*, 021503, DOI: 10.1103/PhysRevE.75.021503.

(12) Kilic, M. S.; Bazant, M. Z.; Ajdari, A. Steric effects in the dynamics of electrolytes at large applied voltages. I. Double-layer charging. *Physical Review E* **2007**, *75*, 021502, DOI: 10.1103/PhysRevE.75.021502.

(13) Bazant, M. Z.; Chu, K. T.; Bayly, B. J. Current-Voltage Relations for Electrochemical Thin Films. *SIAM Journal on Applied Mathematics* **2005**, *65*, 1463–1484, DOI: 10.1137/040609938.

(14) Nørskov, J. K.; Abild-Pedersen, F.; Studt, F.; Bligaard, T. Density functional theory in surface chemistry and catalysis. *Proceedings of the National Academy of Sciences* **2011**, *108*, 937–943, DOI: 10.1073/pnas.1006652108.

(15) Seh, Z. W.; Kibsgaard, J.; Dickens, C. F.; Chorkendorff, I.; Nørskov, J. K.; Jaramillo, T. F. Combining theory and experiment in electrocatalysis: Insights into materials design. *Science* **2017**, *355*, DOI: 10.1126/science.aad4998.

(16) Chandler, D. Electron transfer in water and other polar environments, how it happens. Classical and Quantum Dynamics in Condensed Phase Simulations. 2010; pp 25–49, DOI: 10.1142/9789812839664_0002.

(17) Dou, W.; Nitzan, A.; Subotnik, J. E. Surface hopping with a manifold of electronic states. II. Application to the many-body Anderson-Holstein model. *Journal of Chemical Physics* **2015**, *142*, DOI: 10.1063/1.4908034.

(18) Dou, W.; Nitzan, A.; Subotnik, J. E. Surface hopping with a manifold of electronic states. III. Transients, broadening, and the Marcus picture. *The Journal of Chemical Physics* **2015**, *142*, 234106, DOI: 10.1063/1.4922513.

(19) Marcus, R. A. Exchange reactions and electron transfer reactions including isotopic exchange. Theory of oxidation-reduction reactions involving electron transfer. Part 4.A statistical-mechanical basis for treating contributions from solvent, ligands, and inert salt. *Discuss. Faraday Soc.* **1960**, *29*, 21–31, DOI: 10.1039/DF9602900021.

(20) Warshel, A. Dynamics of reactions in polar solvents. Semiclassical trajectory studies of electron-transfer and proton-transfer reactions. *The Journal of Physical Chemistry* **1982**, *86*, 2218–2224.

(21) Hwang, J. K.; Warshel, A. Microscopic examination of free-energy relationships for electron transfer in polar solvents. *Journal of the American Chemical Society* **1987**, *109*, 715–720.

(22) Blumberger, J.; Sprik, M. *Computer Simulations in Condensed Matter Systems: From Materials to Chemical Biology Volume 2*; Springer, 2006; pp 481–506.

(23) Willard, A. P.; Reed, S. K.; Madden, P. A.; Chandler, D. Water at an electrochemical interfacea simulation study. *Faraday Discuss.* **2009**, *141*, 423–441, DOI: 10.1039/B805544K.

(24) Coffman, A. J.; Harshan, A. K.; Hammes-Schiffer, S.; Subotnik, J. E. Modeling Electron Transfer in Diffusive Multidimensional Electrochemical Systems. *The Journal of Physical Chemistry C* **2019**, *123*, 13304–13317, DOI: 10.1021/acs.jpcc.9b02068.

(25) Chapman, D. L. LI. A contribution to the theory of electrocapillarity. *The London, Edinburgh, and Dublin Philosophical Magazine and Journal of Science* **1913**, *25*, 475–481.

(26) Stojek, Z. In *Electroanalytical Methods: Guide to Experiments and Applications*; Scholz, F., Bond, A., Compton, R., Fiedler, D., Inzelt, G., Kahlert, H., Komorsky-Lovrić, Š., Lohse, H., Lovrić, M., Marken, F., Neudeck, A., Retter, U., Scholz, F., Stojek, Z., Eds.; Springer Berlin Heidelberg: Berlin, Heidelberg, 2010; pp 3–9, DOI: 10.1007/978-3-642-02915-8_1.

(27) Nitzan, A. *Chemical Dynamics in Condensed Phases: Relaxation, Transfer and Reactions in Condensed Molecular Systems*; Oxford university press, 2006.

(28) Morgan, J. D.; Wolynes, P. G. Adiabaticity of electron transfer at an electrode. *The Journal of Physical Chemistry* **1987**, *91*, 874–883, DOI: 10.1021/j100288a023.

(29) Chakravarti, N.; Sebastian, K. Electrochemical electron transfer: a diffusion-reaction equation approach. *Chemical Physics Letters* **1992**, *193*, 456–460.

(30) Mahon, P. J.; Myland, J. C.; Oldham, K. B. A fresh approach to voltammetric modelling. *Journal of Electroanalytical Chemistry* **2002**, *537*, 1–5.

(31) Ouyang, W.; Saven, J. G.; Subotnik, J. E. A Surface Hopping View of Electrochemistry: Non-Equilibrium Electronic Transport through an Ionic Solution with a Classical Master Equation. *The Journal of Physical Chemistry C* **2015**, *119*, 20833–20844.

(32) Ouyang, W.; Subotnik, J. E. The dynamics of charge transfer with and without a barrier: A very simplified model of cyclic voltammetry. *The Journal of Chemical Physics* **2017**, *146*, 174103.

(33) Jortner, J. Temperature dependent activation energy for electron transfer between biological molecules. *The Journal of Chemical Physics* **1976**, *64*, 4860–4867.

(34) Schmickler, W. A unified model for electrochemical electron and ion transfer reactions. *Chemical Physics Letters* **1995**, *237*, 152–160.

(35) Kornyshev, A.; Kuznetsov, A.; Ulstrup, J. Effect of overpotential on the electronic tunnel factor in diabatic electrochemical processes. *The Journal of Physical Chemistry* **1994**, *98*, 3832–3837.

(36) Sutin, N. Theory of electron transfer reactions: insights and hindsights. *Progress in Inorganic Chemistry: An Appreciation of Henry Taube* **1983**, 441–498.

(37) Hopfield, J. Electron transfer between biological molecules by thermally activated tunneling. *Proceedings of the National Academy of Sciences* **1974**, *71*, 3640–3644.

(38) Fan, F.-R. F.; Yang, J.; Cai, L.; Price Jr, D. W.; Dirk, S. M.; Kosynkin, D. V.; Yao, Y.; Rawlett, A. M.; Tour, J. M.; Bard, A. J. Charge transport through self-assembled monolayers of compounds of interest in molecular electronics. *Journal of the American Chemical Society* **2002**, *124*, 5550–5560.

(39) Holmlin, R. E.; Haag, R.; Chabinyc, M. L.; Ismagilov, R. F.; Cohen, A. E.; Terfort, A.; Rampi, M. A.; Whitesides, G. M. Electron transport through thin organic films in metal- insulator- metal junctions based on self-assembled monolayers. *Journal of the American Chemical Society* **2001**, *123*, 5075–5085.

(40) Newton, M. D. Quantum chemical probes of electron-transfer kinetics: the nature of donor-acceptor interactions. *Chemical Reviews* **1991**, *91*, 767–792.

(41) Seitz-Beywl, J.; Poxleitner, M.; Probst, M.; Heinzinger, K. On the interaction of ions with a platinum metal surface. *International Journal of Quantum Chemistry* **1992**, *42*, 1141–1147.

(42) Katz, J. L.; Rice, S. A.; Choi, S.-i.; Jortner, J. On the excess electron and hole band structures and carrier mobility in naphthalene, anthracene, and several polyphenyls. *The Journal of Chemical Physics* **1963**, *39*, 1683–1697.

(43) Elgrishi, N.; Rountree, K. J.; McCarthy, B. D.; Rountree, E. S.; Eisenhart, T. T.; Dempsey, J. L. A Practical Beginners Guide to Cyclic Voltammetry. *Journal of Chemical Education* **2018**, *95*, 197–206, DOI: 10.1021/acs.jchemed.7b00361.

(44) Deen, W. *Analysis of Transport Phenomena*; Topics in chemical engineering; Oxford University Press, 2012.

(45) Franco, A. A. Multiscale modelling and numerical simulation of rechargeable lithium ion batteries: concepts, methods and challenges. *RSC Advances* **2013**, *3*, 13027, DOI: 10.1039/c3ra23502e.

(46) Frumkin, A.; Petry, O.; Nikolaeva-Fedorovich, N. On the determination of the value of the charge of the reacting particle and of the constant α from the dependence of the rate of electro-reduction on the potential and concentration of the solution. *Electrochimica Acta* **1963**, *8*, 177–192.

(47) Petrii, O. A.; Nazmutdinov, R. R.; Bronshtein, M. D.; Tsirlina, G. A. Life of the Tafel equation: Current understanding and prospects for the second century. *Electrochimica Acta* **2007**, *52*, 3493 – 3504, DOI: https://doi.org/10.1016/j.electacta.2006.10.014.

(48) Tsirlina, G.; Petrii, O.; Nazmutdinov, R.; Glukhov, D. Frumkin correction: microscopic view. *Russian Journal of Electrochemistry* **2002**, *38*, 132–140.

(49) Zagrebin, P. A.; Tsirlina, G. A.; Nazmutdinov, R. R.; Petrii, O. A.; Probst, M. Corrected Marcus plots. *Journal of Solid State Electrochemistry* **2006**, *10*, 157–167.

(50) Rusanova, M. Y.; Tsirlina, G. A.; Nazmutdinov, R. R.; Fawcett, W. R. Role of Charge Distribution in the Reactant and Product in Double Layer Effects: Construction of Corrected Tafel Plots. *The Journal of Physical Chemistry A* **2005**, *109*, 1348–1356, DOI: 10.1021/jp046917s, PMID: 16833451.

(51) Nazmutdinov, R. R.; Glukhov, D. V.; Petrii, O. A.; Tsirlina, G. A.; Botukhova, G. N. Contemporary understanding of the peroxodisulfate reduction at a mercury electrode. *Journal of Electroanalytical Chemistry* **2003**, *552*, 261–278.

(52) Weaver, M. J.; Satterberg, T. L. The position of the reaction site and the relative reactivities of simple outer-and inner-sphere electrode reactions. The reduction of some chromium (III) amine complexes at mercury electrodes. *The Journal of Physical Chemistry* **1977**, *81*, 1772–1783.

(53) Parsons, R. The Transfer Coefficient in Electrode Reactions. *Croatica Chemica Acta* **1970**, *42*, 281–291.

(54) Fawcett, W. The location of the reaction site and discreteness-of-charge effects in electrode kinetics. *Canadian Journal of Chemistry* **1981**, *59*, 1844–1853.

(55) Reis, J. C. R. Thermodynamic analysis of the symmetry factor and the transfer coefficient in electrode kinetics. *Journal of The Electrochemical Society* **1997**, *144*, 2404–2409.

(56) Fawcett, W. R.; Chavis, G. J.; Hromadová, M. Charge distribution effects in polyatomic reactants involved in simple electron transfer reactions. *Electrochimica Acta* **2008**, *53*, 6787–6792.

(57) Schiffer, Z. J.; Lazouski, N.; Corbin, N.; Manthiram, K. Nature of the First Electron Transfer in Electrochemical Ammonia Activation in a Nonaqueous Medium. *The Journal of Physical Chemistry C* **2019**, *123*, 9713–9720, DOI: 10.1021/acs.jpcc.9b00669.

(58) Fawcett, W.; Mackey, M. The electroreduction of peroxydisulphate anion in formamide. *Journal of Electroanalytical Chemistry and Interfacial Electrochemistry* **1970**, *27*, 219–231.

(59) Smit, W.; Hoogland, J. The mechanism of the anodic formation of the peroxodisulphate ion on platinumIV. influence of alkali-metal cations. *Electrochimica Acta* **1971**, *16*, 981–993.

(60) Lust, E.; Truu, R.; Lust, K. Electroreduction of peroxodisulfate anion at Bi (111) single-crystal plane electrode. *Russian Journal of Electrochemistry* **2000**, *36*, 1195–1202.

(61) Nazmutdinov, R.; Glukhov, D.; Tsirlina, G.; Petrii, O. Molecular description of the persulfate ion reduction on a mercury electrode. *Russian journal of electrochemistry* **2002**, *38*, 720–731.

(62) Dickinson, E. J.; Compton, R. G. Influence of the diffuse double layer on steady-

state voltammetry. *Journal of Electroanalytical Chemistry* **2011**, *661*, 198 – 212, DOI: https://doi.org/10.1016/j.jelechem.2011.08.002.

(63) Fawcett, W. The effect of ionic size in the double layer on the kinetics of electrode reactions. *Journal of Electroanalytical Chemistry and Interfacial Electrochemistry* **1969**, *22*, 19–28.

(64) Lin, C.; Compton, R. G. Understanding mass transport influenced electrocatalysis at the nanoscale via numerical simulation. *Current Opinion in Electrochemistry* **2018**, DOI: https://doi.org/10.1016/j.coelec.2018.08.001.

Graphical TOC Entry